Liquid Crystals
Publication details, including instructions for authors and subscription information:
http://www.informaworld.com/smpp/title~content=t713926090

Liquid crystal dimers possessing chiral rod-like anisometric segments: synthesis, characterization and electro-optic behaviour

Channabasaveshwar V. Yelamaggad[a]; Indudhara Swamy Shashikala[a]; Uma S. Hiremath[a]; Doddamane S. Shankar Rao[a]; Subbarao Krishna Prasad[a]
[a] Centre for Liquid Crystal Research, Jalahalli, Bangalore 560 013, India

To cite this Article Yelamaggad, Channabasaveshwar V. , Shashikala, Indudhara Swamy , Hiremath, Uma S. , Rao, Doddamane S. Shankar and Prasad, Subbarao Krishna(2007) 'Liquid crystal dimers possessing chiral rod-like anisometric segments: synthesis, characterization and electro-optic behaviour', Liquid Crystals, 34: 2, 153 — 167
To link to this Article: DOI: 10.1080/02678290601137585
URL: http://dx.doi.org/10.1080/02678290601137585

Liquid Crystals, Vol. 34, No. 2, February 2007, 153–167

Liquid crystal dimers possessing chiral rod-like anisometric segments: synthesis, characterization and electro-optic behaviour

CHANNABASAVESHWAR V. YELAMAGGAD*, INDUDHARA SWAMY SHASHIKALA, UMA S. HIREMATH, DODDAMANE S. SHANKAR RAO and SUBBARAO KRISHNA PRASAD

Centre for Liquid Crystal Research, Jalahalli, Bangalore 560 013, India

(*Received 11 April 2006; in final form 2 October 2006; accepted 5 October 2006*)

Several new optically active liquid crystal dimers comprising pro-mesogenic cholesterol and a chiral diphenylacetylene (tolane) segment, covalently linked in an end-to-end fashion through a flexible spacer, have been synthesized and investigated for their mesomorphic behaviour with the aid of optical, calorimetric and X-ray diffraction studies. Five unsymmetrical dimers, designed on the basis of recent work, involve molecular structural variations of the tolane mesogenic entity with a view to stabilizing a wide thermal range smectic A (SmA) phase featuring the electroclinic effect. Three different chiral chains, namely, (*S*)-1-methylheptyloxy, (*S*)-2-methylbutyloxy, (3*S*)-3,7-dimethyloctyloxy, with or without polar (nitro or fluoro) lateral substituents, were incorporated, while keeping the length (C_6) of the spacer constant. As expected, all the dimers exhibited a SmA phase. A few also showed chiral nematic (N*) and/or twist grain boundary and/or chiral smectic C (SmC*) phases. Remarkably, some of these oligomesogens, upon melting, had a stable SmA phase over a wide thermal interval (100–150°C); this state seems to be stable for a long period of time. Electro-optic studies, including optical tilt angle as well as temporal response as a function of temperature, were carried out in the SmA phase. The SmC* phase was also investigated for its electrical switching and optical tilt angle, as well as spontaneous polarization as a function of temperature. These studies showed that the mesophase response to an applied field is weak and is independent of variations in the dimer investigated.

1. Introduction

In recent times, liquid crystal (LC) dimers have been the focus and targets of many researchers because they exhibit remarkable and quite different phase transitional properties to conventional LCs [1]; they can also be regarded as model compounds for main chain LC polymers [2]. A symmetrical or unsymmetrical dimer is formed when two chemically identical or non-identical anisometric segments, respectively, are connected covalently through a flexible spacer [1, 2]. Of the variety of unsymmetrical dimeric architectures known, dimers consisting of a cholesteryl ester entity joined axially to a non-chiral segment have attracted a great deal of attention [3–14]. This is because such oligomesogens exhibit a remarkable thermal behaviour, viz: incommensurate smectic A mesophase [3], anomalies of periodicity in twist grain boundary (TGB) phases [5], reentrant TGB phases [12], etc. It would clearly be of much interest to introduce chirality into the non-cholesteryl mesogenic unit as well, and to evaluate its influence on thermal behaviour in particular, with a view to exploring the possibility of obtaining technologically important mesophases in these systems. With this aim in mind, we have recently attached a diphenylacetylene (tolane) mesogenic entity having a (1*S*)-1-methylheptyloxy chain to a cholesteryl ester segment through a C_6-spacer [13]. Interestingly, the resultant dimer, hereafter referred to as **1** (see scheme 1), was found to exhibit the smectic A (SmA) phase over a temperature range of ~150°, well below and above room temperature. Electro-optic studies showed that it

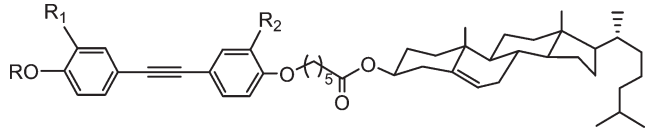

1 : R = (*S*)-1-Methylheptyloxy; $R_1 = R_2 = H$
1a : R = (*S*)-1-Methylheptyloxy; $R_1 = NO_2$; $R_2 = H$
1b : R = (*S*)-1-Methylheptyloxy; $R_1 = F$; $R_2 = H$
2a : R= (*S*)-2- Methylbutyloxy; $R_1 = R_2 = H$
2b : R= (2)-2- Methylbutyloxy; $R_1 = H$; $R_2 = NO_2$
3 : R= (3*S*)-3,7-Dimethyloctyloxy; $R_1 = R_2 = H$

Scheme 1. Molecular structures of liquid crystal dimers **1** and **1a–3**.

*Corresponding author. Email: yelamaggad@yahoo.com

Liquid Crystals
ISSN 0267-8292 print/ISSN 1366-5855 online © 2007 Taylor & Francis
http://www.tandf.co.uk/journals
DOI: 10.1080/02678290601137585

exhibits an observable electroclinic effect over this entire temperature range. However, the electroclinic tilt angle was small and the response time slower. These results prompted us to modify the structure of dimer **1** with a view to improving these parameter values.

In the electroclinic effect, an electric field applied parallel to the plane of smectic layers couples to the transverse molecular dipole moment leading to a tilt of molecules with respect to the layer normal and in a plane perpendicular to the electric field (figure 1) [14]. This phenomenon is of much interest because its switching is many times faster than Goldstone-mode switching in ferroelectric LCs. Thus electroclinic materials are promising for a variety of electro-optical device applications [15] as well as in spatial light modulation having grey scale capabilities [16]. For such applications, the optically active LC must have chemical stability, large tilt angles, fast switching times, and a wide thermal range down to sub-ambient temperatures of the SmA phase. The design of such chiral smectic A LCs clearly requires a basic understanding of the molecular structure–property relationship. In contrast to rod-like ferroelectric LCs, electroclinic materials seemingly have not been investigated with regard to simple structure-property relationships. However, it appears that the position of the chiral centre in the alkyl chain, and thus its distance from the rigid core, as well as the length of the chain appear to influence the magnitude of the electroclinic effect in conventional rod-like LCs [7]. The introduction of polar groups onto the mesogenic core also seems to improve the electroclinic effect [17–19]. Furthermore, surprisingly, in this context LC dimers have been explored only briefly [13, 20–22]. For example, apart from our recent work, a chiral symmetrical dimer possessing ferroelectric mesogens joined by a dimethylsiloxane flexible spacer has been reported to display pronounced ferroelectric as well as electroclinic behaviour [20]. There is thus a need to initiate a systematic study on chiral LC dimers exhibiting the SmA phase and look for the electroclinic effect. To the best of our knowledge such a study has not been undertaken hitherto. In this context, we describe here the synthesis and characterization of several dimers basically designed with a view to improve the electroclinic behaviour of dimer **1**. These studies should primarily provide some insight into the understanding of structure–property relationships. Five new dimers designed with a fixed length of the spacer (pentamethylenecarbonyl, $-(CH_2)_5CO-$) involve variations in (i) the nature and position of polar ($-NO_2$ and $-F$) substituents; (ii) the location of the chiral centre; and (iii) the length of the chiral chain.

2. Synthesis and molecular structural characterization

The synthetic strategy for chiral LC dimers **1a**, **1b**, **2a**, **2b** and **3** was similar to that described for the dimer **1** [13], and accordingly the requisite intermediates **4a, b**, **5a–d** **6a–d** and **7a–d** were prepared as depicted in scheme 2. Phenols **8a–b** were first *O*-alkylated with either (*R*)-octan-2-ol or (*S*)-2-methyl-1-butanol under Mitsunobu reaction conditions to obtain the ethers **7a–c**. Ether **7d** was prepared by *O*-alkylation of phenol **8c** with (*S*)-1-bromo-3,7-diemthyloctane using the Williamson ether synthesis procedure. Subsequently, these ethers **7a–d** were coupled with 2-methyl-3-butyn-2-ol under palladium-catalysed (Sonogashira) reaction conditions to obtain protected acetylenes **6a–d** (68–85 % yield), which upon refluxing with potassium hydroxide in toluene generated the key intermediates **5a–d** in almost quantitative yield. Cholesterol derivatives **4a** and **4b** required in the final coupling were obtained in 60 and 58 % yield, respectively, by the *O*-alkylation of substituted phenols with cholesteryl 6-bromohexanoate

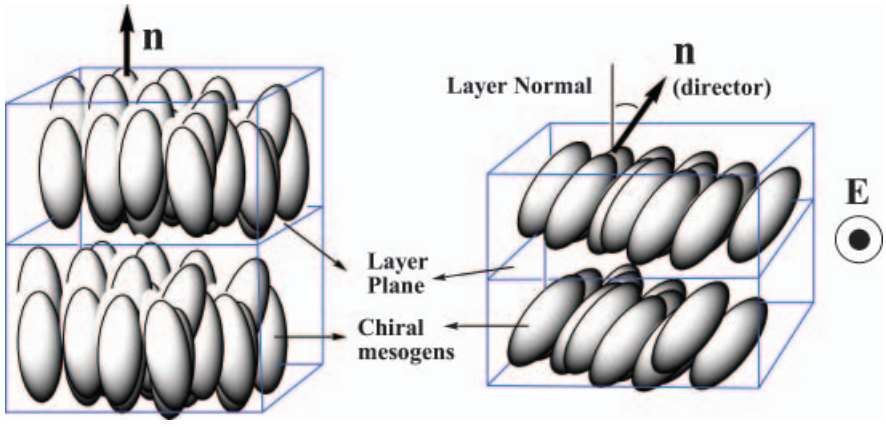

Figure 1. Schematic representation of the SmA phase possessing chiral rod-like anisometric molecules: (*a*) orthogonal layered geometry; (*b*) tilted layered structure (electroclinic effect) obtained by the application of an electric field along the layer planes.

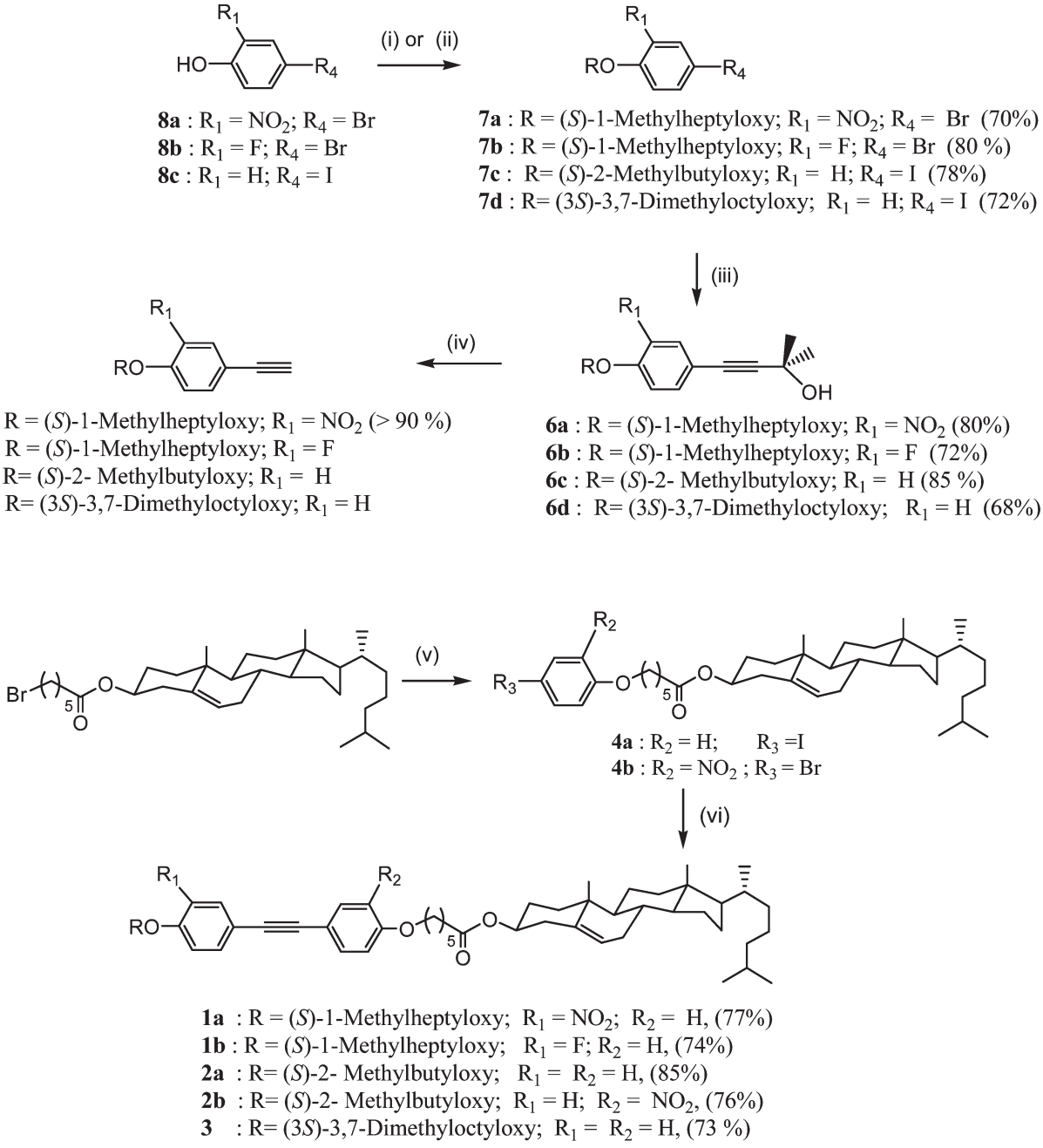

8a : $R_1 = NO_2$; $R_4 = Br$
8b : $R_1 = F$; $R_4 = Br$
8c : $R_1 = H$; $R_4 = I$

7a : R = (*S*)-1-Methylheptyloxy; $R_1 = NO_2$; $R_4 =$ Br (70%)
7b : R = (*S*)-1-Methylheptyloxy; $R_1 = F$; $R_4 = Br$ (80 %)
7c : R= (*S*)-2-Methylbutyloxy; $R_1 =$ H; $R_4 = I$ (78%)
7d : R= (3*S*)-3,7-Dimethyloctyloxy; $R_1 =$ H; $R_4 = I$ (72%)

5a : R = (*S*)-1-Methylheptyloxy; $R_1 = NO_2$ (> 90 %)
5b : R = (*S*)-1-Methylheptyloxy; $R_1 = F$
5c : R= (*S*)-2- Methylbutyloxy; $R_1 =$ H
5d : R= (3*S*)-3,7-Dimethyloctyloxy; $R_1 = H$

6a : R = (*S*)-1-Methylheptyloxy; $R_1 = NO_2$ (80%)
6b : R = (*S*)-1-Methylheptyloxy; $R_1 = F$ (72%)
6c : R= (*S*)-2- Methylbutyloxy; $R_1 =$ H (85 %)
6d : R= (3*S*)-3,7-Dimethyloctyloxy; $R_1 = H$ (68%)

4a : $R_2 = H$; $R_3 = I$
4b : $R_2 = NO_2$; $R_3 = Br$

1a : R = (*S*)-1-Methylheptyloxy; $R_1 = NO_2$; $R_2 =$ H, (77%)
1b : R = (*S*)-1-Methylheptyloxy; $R_1 = F$; $R_2 = H$, (74%)
2a : R= (*S*)-2- Methylbutyloxy; $R_1 = R_2 = H$, (85%)
2b : R= (*S*)-2- Methylbutyloxy; $R_1 = H$; $R_2 = NO_2$, (76%)
3 : R= (3*S*)-3,7-Dimethyloctyloxy; $R_1 = R_2 = H$, (73 %)

Scheme 2. Reagent and conditions: (i) 2(*R*)-Octanol +**8a** (for **7a**), or 2(*R*)-octanol +**8a** (for **7b**), or 2(*S*)-methylbutanol+**8c** (for **7c**), Ph_3P, DEAD, THF, 0°C to r.t., 12 h, 68–70%; (ii) (*S*)-1-bromo-3,7-dimethyloctane+**8c** (for **7d**), K_2CO_3, acetone, reflux, 16 h, >90; (iii) 2-methyl-3-butyn-2-ol, CuI, Ph_3P, $(Ph_3P)_2PdCl_2$, THF, Et_3N, 85°C, 12 h, 68–85%; (iv) KOH, toluene, reflux, 1 h, >90%; (v) 4-iodophenol or 4-bromo-2-nitrophenol, K_2CO_3, DMF, 85°C, 16 h, >90%; (vi) **5a**+**4a** (for **1a**) or **5b**+**4a** (for **1b**) or **5c**+**4a** (for **2a**) or **5c**+**4b** (for **2b**) or **5d**+**4a** (for **3**) and CuI, Ph_3P, $(Ph_3P)_2PdCI_2$, THF Et_3N, 85°C, 12 h.

[13] by Williamson ether synthesis methods. In the final step, cholesteryl esters **4a** and **4b** were coupled with acetylenes **5a–d** to obtain the target molecules **1a**, **1b**, **2a**, **2b**, **3** (73–85 % yield) as crystalline compounds.

The molecular structures of the dimers synthesized were assessed with the help of standard spectroscopic and elemental analyses. Some of the important features obtained in the IR and NMR spectra are highlighted as follows. The IR spectra display bands in the region of ν_{max}/cm^{-1} 2932–2945, 1727–1740 and 1608–1618, related to C–H (paraffinic), carbonyl (C=O of ester) and C=C (aromatic) stretching vibrations respectively.

In the ^{1}H NMR spectra, the olefinic, methine of ester and oxymethylene of paraffinic chain protons resonate in the region of δ 5.36–5.37, 4.5–4.65 and 3.85–4 as a broad doublet (d), multiplet (m) and triplet (t), respectively. The spectral pattern in the region δ 0–2 was found to be complex; however the resonances due to protons of five methyl groups of cholesterol could be seen. The *gem*-dimethyl protons appear as two doublets, resonating sharply at δ 0.85 and 0.87 in all cases. The protons of two methyl groups attached to quaternary carbon centres appear as two singlets in the region of δ 0.99–1.01 and 0.66–0.67. The protons of a methyl group attached to a methine carbon appear as a doublet in the region of δ 0.89–0.91. As expected, in the ^{13}C NMR spectra, the signals due to carbons appearing at lower as well as higher (down the chroform peaks) frequency are found to be consistent with the proposed structure. For example, the C=O carbon resonates in the range of δ 172.9–173 whereas two sp-hybridized (acetylene) carbons appear at δ 88.7–90.2 and 85.5–87.9 (see §6).

3. Mesomorphic behaviour

The unsymmetrical dimers were investigated for liquid crystalline behaviour with the help of a polarizing optical microscope (POM) in conjunction with a programmable hot stage, as well as by differential scanning calorimetry (DSC). The structure of the mesophases and electrical switching behaviour, respectively, were assessed by powder X-ray diffraction (XRD) and electro-optical studies. For the POM studies, in addition to untreated glass slides, substrates treated for planar or homeotropic alignment were employed. The thermal behaviour data are gathered in table 1. As can be seen, all the dimers display the smectic A phase, established on the basis of its characteristic focal-conic fan/pseudoisotropic textures coexisting for samples placed between untreated glass slides. Interestingly, the dimers **1a** and **1b** stabilize the SmA phase over a wide temperature range as evidenced by both POM and DSC studies, as described as below.

Dimers **1a** and **1b** placed on slides treated for planar orientation, on heating, transform into a SmA phase with its characteristic fan shaped texture. Additionally for dimer **1b**, the chiral nematic phase with its typical planar texture that on mechanical shear yields an oily streak texture, figure 2(*a*), was observed. On cooling from the N* or isotropic phase, transition to the SmA phase occurred at about 110°C (ΔH=1.3 J g^{-1}) and

Table 1. Transition temperatures (°C)[a] and enthalpies (J gm^{-1}), in brackets, of the unsymmetrical dimers. Cr=crystal; M_x=unknown mesophase; SmC*=chiral smectic C phase; SmA=smectic A phase; TGB=twist grain boundary phase with either SmA or SmC blocks; N*=chiral nematic phase; I=isotropic liquid state.

Compound	Cr	Heating Cooling	M_x	Heating Cooling	SmC*	Heating Cooling	SmA	Heating Cooling	TGB	Heating Cooling	N*	Heating Cooling	I
1a	•	86.4[b] (34.9)	—	—	—	—	•	111.2 (1.3)	—	—	•	113.1 (1.2)	•
		[c]						110.4 (1.3)				112.6 (1.2)	
1b	•	84.4 (45.9)	—	—	—	—	•	145.6 (10.6)	—		—	—	•
		[c]						144.5[d] (10.2)					
2a	•	120.8 (32)				—	•	159.2 (1.2)	•	[d, e]	•	182.9 (4.2)	•
		51.4 (5)	•	63.1 (1.1)				158.5 (1.2)				180.7 (4.2)	
2b	•	138.6 (37.9)	—		—		•	—	—	—	•	143.8 (3.5)	•
		[c]						134.1 (4.9)				143.1 (3.4)	
3	•	92.8 (41.8)	—		•	99.9[d] —	•	168.3 (11.3)	—		—		•
		45[f]				99.5[d] —		166.5 (11.1)					

[a]Peak temperatures in the DSC thermograms obtained during the first heating and cooling cycles at 5°C min^{-1}. [b]An additional crystal to crystal transition has been observed at 60.1 (5.4). [c]Step-like variations occur for the compounds **1a**, **1b** and **2b** at −2, −11 and 5.7°C, respectively which could be due to either a transition from the SmA to another mesophase or a glass transition that exists till −60°C; on subsequent cooling these step-like variations appear at −8, −5 and 10.8°C respectively. [d]The phase transition was observed under polarizing microscope but too weak to see in DSC. [e]TGB is a transient phase. [f]The transition to crystalline phase was seen under the microscope.

144°C (ΔH=10.2 J g^{-1}) for compounds **1a** and **1b** respectively, which remains unchanged down to room temperature. Photomicrographs of the fan-shaped texture obtained at 140°C and room temperature for dimer **1b** are shown in figures 2(*b*) and 2(*c*), respectively. The DSC traces obtained for **1a** and **1b** are shown in figures 3A and 3B, respectively. In the DSC traces obtained in cooling, a step like variation occurs for both dimers **1a** and **1b** at about −2°C (ΔH=1 J g^{-1}) and −11°C (ΔH=0.9 J g^{-1}), respectively, indicating that the SmA phase either freezes into a glassy state or transforms to another mesophase that remains unchanged down to −50°C, the lowest temperature achievable with our experimental set-up. Thus, the temperature range of the SmA phase is about 112 and 155°C for **1a** and **1b** respectively and is comparable to earlier results [13, 23]. On subsequent heating from −50°C, a small rounded peak was seen for both samples **1a** and **1b** at about 1°C and −10°C, respectively, and no other peaks were observed until the SmA–N* and SmA–I transitions, respectively, were reached. These transitions were highly reproducible during repeated heating and cooling cycles. Interestingly, no sign of crystallization was noticed, even after todays at room temperature. However, repeated mechanical disturbance does induce crystallization. Thus, dimers **1a** and **1b** form the SmA phase well below and above room temperature, a feature that can be attributed to the proximity of the chiral centre to the tolane core; the presence of a laterally substituted polar group perhaps disfavours the formation of other layered structures such as the chiral smectic C (SmC*) phase. This behaviour is quite remarkable in view of the fact that for their use in any practical applications a wide thermal range of mesophase is an imperative requirement. Furthermore, the existence of the SmA phase below the N* phase for dimer **1a** is of special significance: such a sequence is especially useful from an experimental point of view as it provides a well aligned SmA phase.

Dimer **2a**, having an optically active methylbutyloxy chain showed a polymesomorphic sequence. While cooling from the isotropic phase, between untreated glass slides, it shows a focal-conic texture, which on mechanical shearing furnishes a Grandjean planar texture indicating the presence of the N* phase. On further cooling, the SmA phase appears (through a transient TGB phase), confirmed by microscopic observation of characteristic focal-conic textures in slides treated for planar orientation, and a dark field of view when slides treated for homeotropic orientation were used. The TGB phase showed the filament texture, figure 2(*d*), on heating from the homeotropically oriented SmA phase.

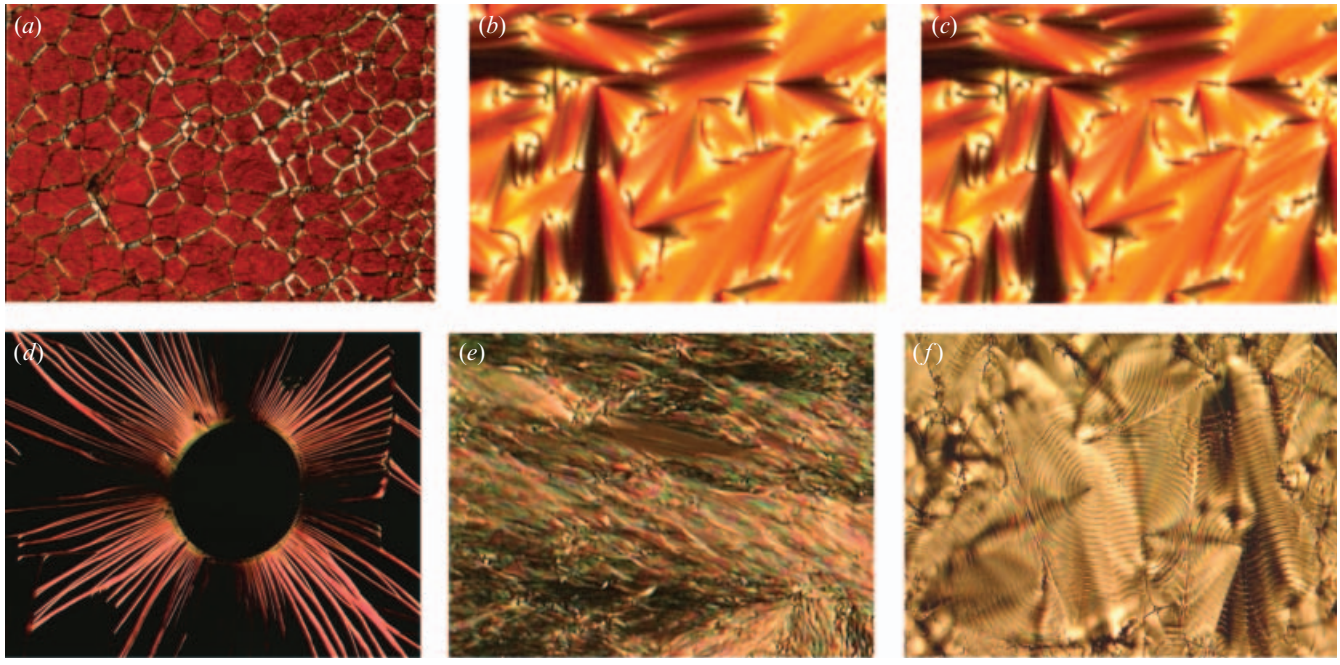

Figure 2. Photomicrographs of the optical textures of different mesophases exhibited by dimers **1a–3**: (*a*) the oily streak texture obtained for the N* phase of **1a** at 112°C; (*b*) and (*c*) the focal-conic texture obtained for the planar SmA phase of dimer **1b** at 140°C and room temperature respectively; (*d*) the filamentary texture seen for the TGB phase on heating **2a** from a homeotropic SmA phase; (*e*) a non-specific texture of the M_x phase observed at 60°C for **2a**; (*f*) the SmC* phase exhibiting dechiralization lines on top of the broken focal-conics seen for **3** at 90°C.

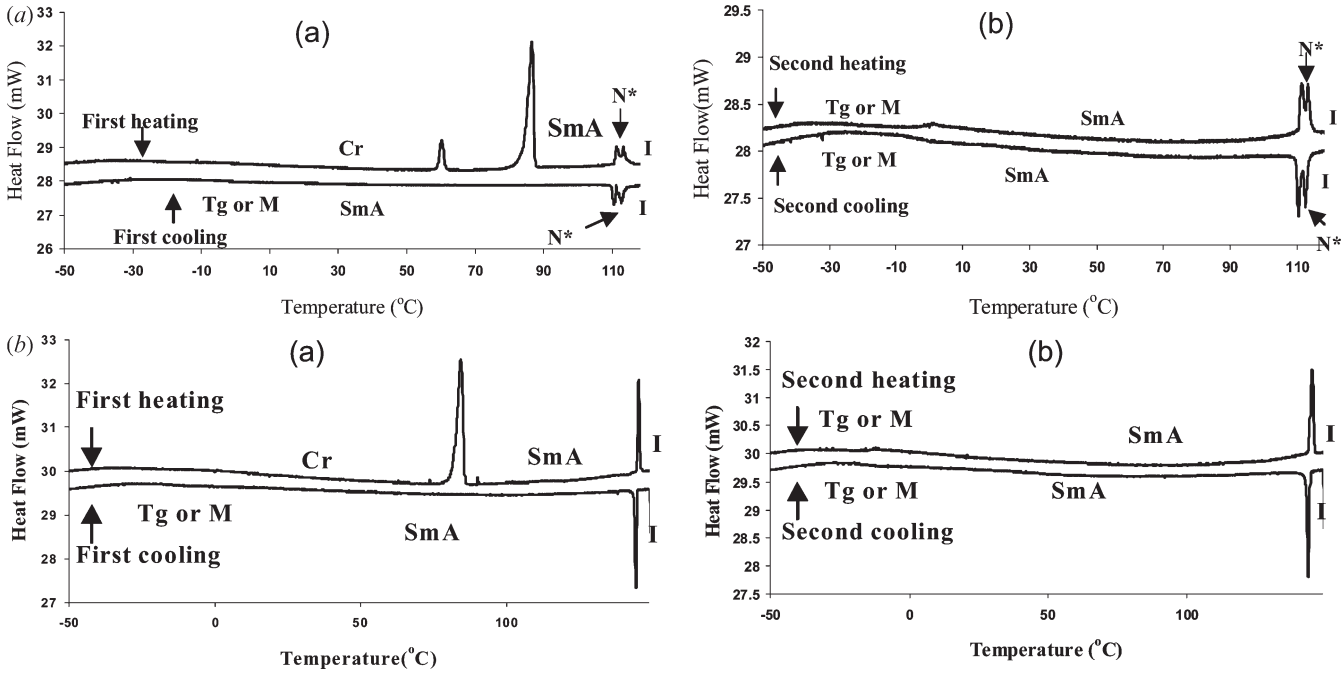

Figure 3. DSC profiles obtained for dimers **1a** (A) and **1b** (B) during the first (*a*) and second (*b*) heating-cooling cycles.

Of course, due to the transient nature of the TGB phase, the N* and SmA phases coexisted along with it; the textures corresponding to these three mesophases exist simultaneously for a short while in both heating and cooling cycles. An unknown mesophase (abbreviated as M_x) also occurs over a short thermal range below the SmA phase. This monotropic phase exhibited a non-specific (smeared focal-conic) texture, figure 2 (*e*), when slides treated for planar geometry were used. In slides treated for homeotropic geometry, the M_x phase initially grows as bâtonnets having dechiralization lines that coalesce to a cloudy texture. Because of its existence over a short range of temperature and the tendency of crystallization, further investigations were not possible.

Compound **2b**, the nitro analogue of **2a**, exhibits the N* phase in addition to a monotropic SmA phase. Remarkably, the SmA phase supercools and stabilizes down to about 6°C. However, both mechanical shear and heating destabilize the SmA phase. Furthermore, in this dimer the N*–I transition temperature is considerably reduced when compared with dimer **2a**, which can be attributed to the presence of polar lateral substitution. Dimer **3**, with a chiral dimethyloctyloxy chain, exhibits enantiotropic SmC* and SmA phase only. In slides treated for planar orientation the SmC* phase exhibited dechiralization lines on top of the focal-conic texture, figure 2 (*f*), while with surfaces treated for homeotropic alignment a cloudy pattern was observed. Thus, as expected, the nature of the chiral chain and polar lateral substituents in the aromatic mesogenic segment of these unsymmetrical dimers markedly influence their thermal behaviour.

4. X-ray diffraction studies

Mesogens having a strongly polar terminal group such as –CN or $–NO_2$ are well known to exhibit different forms of SmA phase, viz. monomolecular-layered SmA_1, partially bilayer SmA_d or true bilayer SmA_2 structures. In particular, the smectic A behaviour of unsymmetric dimers appears rather intriguing [1]. Dimeric molecules add intercalated structures to this variety. For example, within the same series, certain homologues exhibit an intercalated smectic phase in which the layer spacing (*d*) is close to the half the molecular length (*l*), while other homologues form smectic phases in which the periodicity is larger than the molecular length [1]. In order to ascertain the nature of the smectic A phase formed by the unsymmetrical dimers of this study, X-ray powder diffraction studies were carried out on dimers **1a**, **1b** and **3**. The sample under investigation was filled into a Lindemann capillary tube (1 mm diameter) in the isotropic phase and both the ends of tube were flame sealed. The diffraction patterns obtained in the mesophase formed while cooling from the isotropic phase were collected on an image plate.

The X-ray diffractograms obtained in the SmA phases for the dimers **1a**, **1b** and **3** are shown in figures 4, 5 and 6, respectively. For dimer **1a** the X-ray

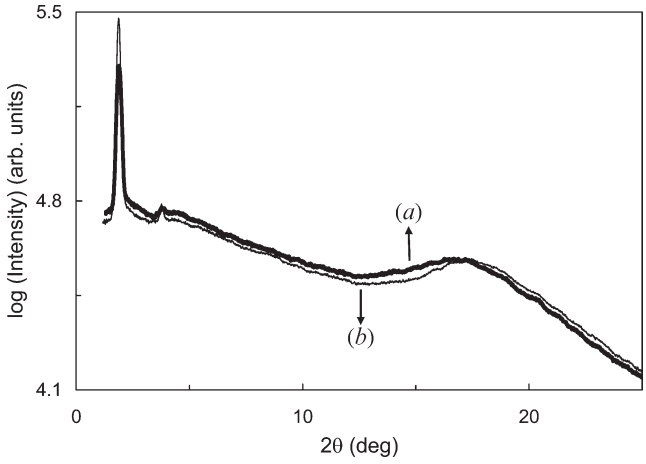

Figure 4. X-ray 1D intensity vs 2θ profile obtained in the SmA phase for dimer **1a** at (*a*) 100°C, (*b*) room temperature (32°C).

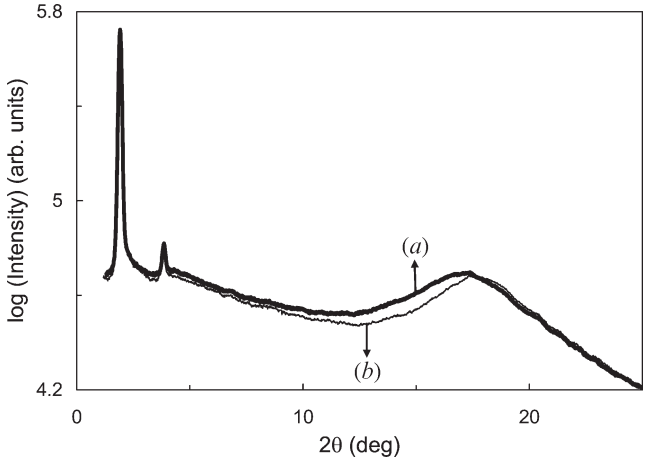

Figure 5. Intensity vs 2θ profile of the XRD patterns obtained in the SmA phase for dimer **1b** at (*a*) 120°C, (*b*) 50°C.

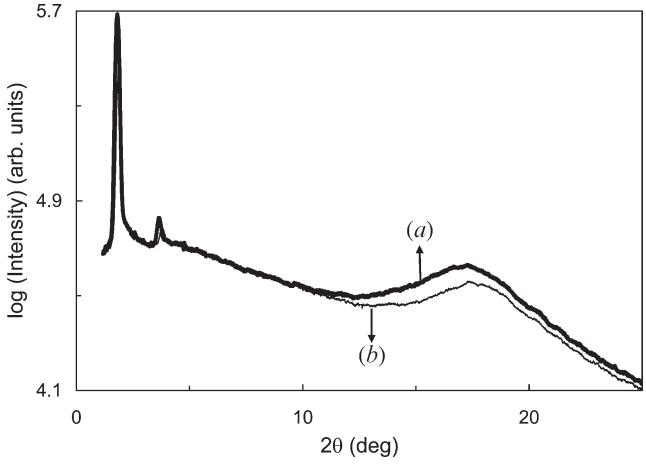

Figure 6. Intensity vs 2θ profile of the XRD patterns obtained in the (*a*) SmA and (*b*) SmC* phases at 130°C and 80°C, respectively, for dimer **3**.

intensity profiles obtained in the smectic A phase at 100°C, as well as at room temperature, are given in figures 4 (*a*) and 4 (*b*), respectively. The diffraction pattern in figure 4 (*a*) shows a sharp reflection in the small angle region with *d* (spacing)-value of 46.7 Å. In the wideangle region a diffuse reflection is seen with spacing of 4.7 Å corresponding to the intermolecular separation within the smectic layer due to the liquid-like positional correlation. The calculated length in the most extended form in the all-*trans* configuration of the molecule (*l*), measured using a Chem3D molecular model is l=46.7 Å. Obviously the value 46.7 Å corresponds to the length of the molecule, with a d/l ratio of 1 which is characteristic of a monolayer smectic A phase. The reflection at 23 Å (d/l=0.49 Å) is the second harmonic and is generally seen in dimeric systems [13]. The diffraction pattern obtained, figure 4 (*b*) for a long-standing sample at room temperature, was found to be almost similar to the profile observed at 100°C. Two reflections are seen in the low angle region with *d*-values of 47.2 and 23.4 Å, respectively, which are slightly higher than those obtained at 100°C and account for the stretching of the alkyl chains. But the important point to note is the diffuse peak seen at 5 Å, indicating liquid-like ordering within the smectic layer. Thus dimer **1a** exhibits a monolayer smectic A phase over a wide thermal range covering room temperature.

Diffractograms of the mesophase obtained for dimer **1b** at 120°C, figure 5 (*a*), and 50°C, figure 5 (*b*), as expected, show two reflections in the small angle region having *d*-values of 46.1/22.9 and 46.7/23.2 Å, respectively. In the wide angle region for both the higher and lower temperature profiles diffuse reflections at about 5.1 and 5 Å were seen, respectively. Thus, the smectic periodicity is approximately equal to the length of the mesogen (46.6 Å) in its all-*trans* conformation as measured using Chem3D software, which supports the monolayer layer arrangement of the molecules in the SmA phase. Dimer **3**, as mentioned earlier, displays SmA and SmC* phases. The X-ray profile obtained in these two phase at 130 and 80°C are depicted in figures 6 (*a*) and 6 (*b*), respectively. The diffractogram of the SmA phase has features similar to those obtained for **1a** and **1b**: two sharp reflections in the small angle region with *d*-values of 48.7 and 24.2 Å, and a wide angle diffuse peak at 5.1 Å. With a molecular length of 48 Å, the d/l ratio is slightly greater than 1, confirming the monolayer nature of the SmA phase for this dimer also. The diffraction pattern appears quantitatively the same in the SmC* phase, figure 6 (*b*), with the exception that the *d*-values of small angle region reflections are decreased to 46.8 and 23.3 Å. Using a simple rigid-rod model, the calculated tilt angle in the SmC* phase is 16°,

a value common in materials exhibiting the SmA–SmC* transition. From these unambiguous characterizations, we can emphasize that all the dimers synthesized in the present investigation display a smectic A phase in which the mesogens are arranged in singular molecular layers.

5. Electrical switching studies

The smectic A and/or chiral smectic C phases formed by these dimers were investigated for their electrical switching properties. In the context of practical applications based on the electroclinic effect, it is an advantage to have a material that exhibits a wide temperature range for the SmA phase. Owing to the stabilization of this mesophase over a wide temperature range, including room temperature, detailed electro-optic studies were performed on dimers **1a** and **1b**. In addition, dimer **3** was also investigated for its electro-optic response. The samples were sandwiched between indium tin oxide (ITO)-coated glass plates pre-treated with a polyimide solution and unidirectionally rubbed for homogeneous alignment. The sample was filled into the cells in the isotropic phase by capillary action and cooled slowly into the mesophase. In the case of dimers **1a** and **1b**, in which the methyl group being close to the lateral substituent hinders its rotation about the long axis of the molecule, one would expect a large dipolar coupling and hence large tilt angles. The electro-optical response profile obtained for dimer **1a** at 80°C under a 200 Hz, 9.5 V μm^{-1} square wave field is shown in figure 7 (*a*). The response time (τ), defined as the time for the transmitted intensity to increase from 10% to 90% of the maximum value, is 250 μs and is similar to values seen for room temperature dimeric electroclinic material reported earlier from this laboratory [13]. For this dimer, the optical response is seen for only a quite high electric field, indicating that the magnitude of the electroclinic effect is much weaker, contrary to our expectation that the presence of a polar lateral substituent should enhance the effect. Thus, a slight variation in the molecular structure of **1** causes a dramatic variation in the electroclinic effect.

Figure 7 (*b*) shows the optical response obtained for dimer **1b** at 80°C under a 200 Hz, 8.7 V μm^{-1} square wave field. Similar results were obtained for dimer **3** under a 200 Hz, 8.6 V μm^{-1} square wave field at 120°C,

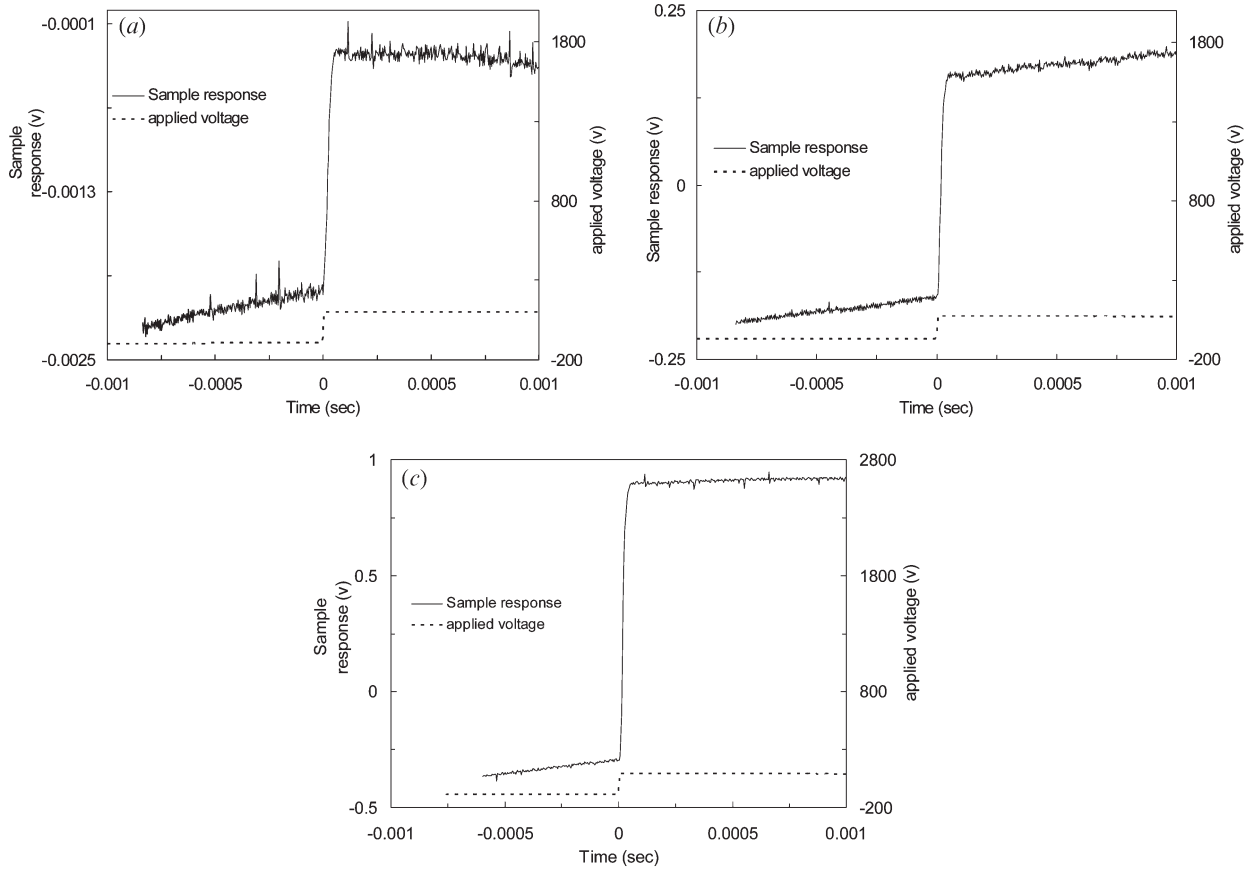

Figure 7. Electro-optic response obtained on application of a square wave electric field to the dimers: (*a*) **1a** at 80°C; (*b*) **1b** at 80°C; (*c*) **3** at 120°C.

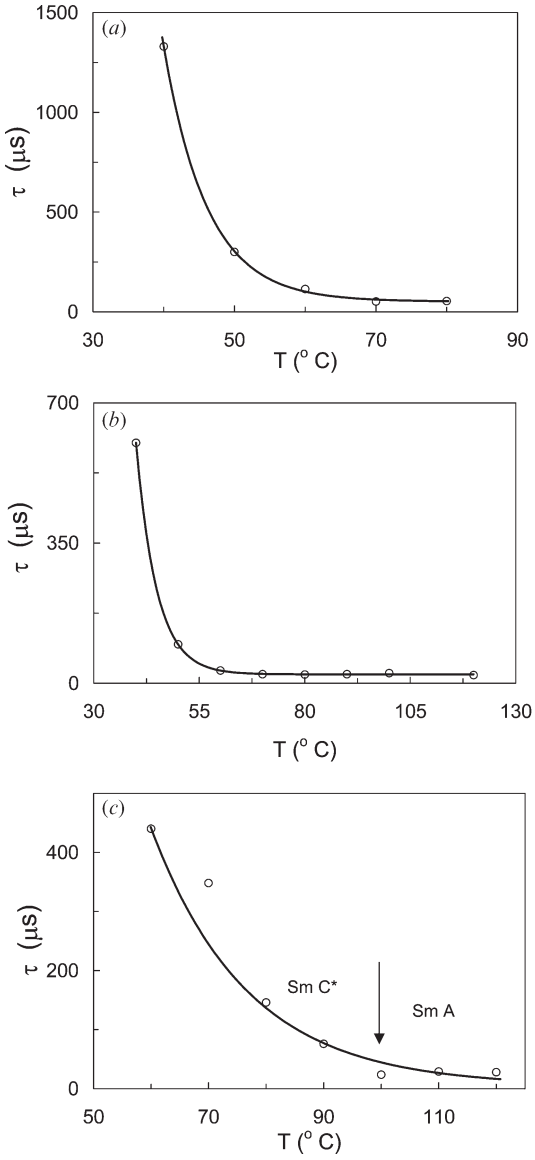

Figure 8. Optical response as a function of temperature under a square wave electric field of about 9 V μm^{-1}: field (*a*) **1a**; (*b*) **1b**; (*c*) **3** (solid line is guide to the eye).

figure 7 (*c*)). Figures 8 (*a*) and 8 (*b*) show the plots of switching time (τ) as a function of temperature in the SmA phase for dimers **1a** and **1b**, respectively. It can be seen that the dimer **1b** having a fluorine lateral substitution, for example at 40°C, has a faster response. For the dimer **3**, τ as a function of temperature was measured in both SmA and SmC* phases, figure 8 (*c*). As expected, for all the dimers the response time increases with decrease in temperature.

For dimers **1b** and **3** the optical tilt angle was measured as a function of temperature in the SmA and/or SmC* phase and the corresponding profiles obtained are shown in figures 9 (*a*) and 9 (*b*), respectively. The

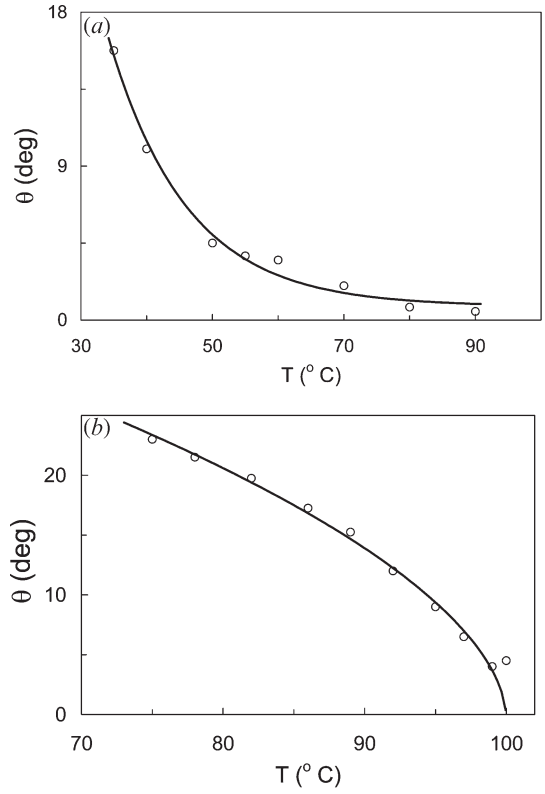

Figure 9. Optical tilt angle as a function of temperature obtained under a square wave field of 9 V μm^{-1} (*a*) **1b** in the SmA phase; (*b*) **3** in the SmC* phase (solid line is guide to the eye).

behaviour observed is characteristic of a phase transition from orthogonal to tilted smectic phase. The electrical response to an applied triangular wave field in the SmC* phase of dimer **3** at 75°C is given in figure 10. The current profile exhibits one peak per half period of the applied field, indicating the ferroelectric

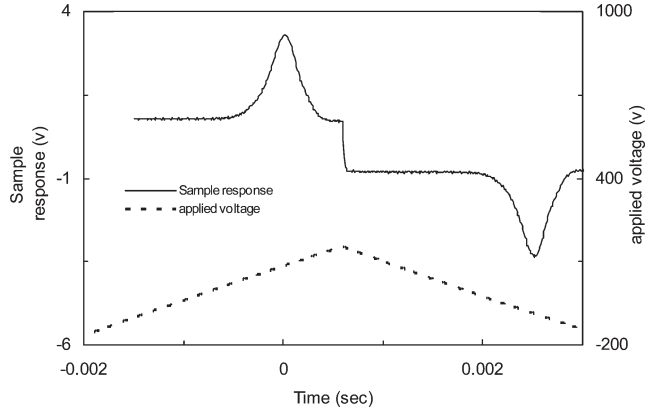

Figure 10. Current response peak in the SmC* phase of dimer **3** obtained at 75°C on applying a triangular wave field (200 Hz, 81.8 V); polarization value ($\mathbf{P}_s$)=16 nC cm^{-2}.

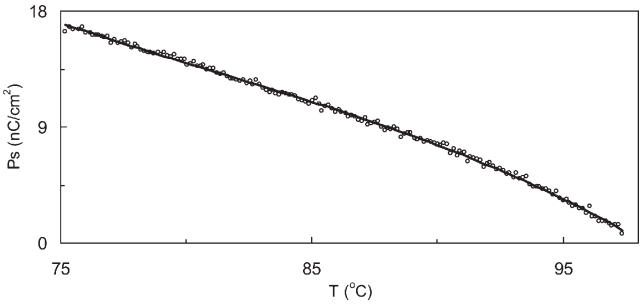

Figure 11. Temperature variation of spontaneous polarization ($\mathbf{P}_s$) obtained in the SmC* phase for dimer **3** (solid line is guide to the eye).

switching characteristic of the SmC* phase. The temperature dependence of spontaneous polarization ($\mathbf{P}_s$) obtained by integrating the area under the peaks is shown in figure 11. The observed low value of $\mathbf{P}_s$ can be attributed to the presence of a bulky cholesteryl ester entity in the molecular structure.

6. Experimental

6.1. *General information*

Cholesterol, 6-bromohexanoic acid, 2-nitro-4-bromophenol and 4-bromo-2-fluorophenol were purchased from Aldrich Chemical Company and used as received. Solvents used in reactions were purified and dried by standard methods. The crude samples were purified by column chromatography using either silica gel (400 mesh) or neutral aluminium oxide as a stationary phase. Thin layer chromatography (TLC) was performed on aluminium sheets pre-coated with silica gel (Merck, Kieselge 60, F_{254}). The absorption spectra were recorded on a Perkin-Elmer Lambda 20 UV-Vis spectrometer. IR spectra were recorded using a Perkin-Elmer Spectrum 1000 FTIR spectrometer. ^{1}H NMR spectra were recorded using either a Bruker AMX-400 (400 MHz) or a Bruker Aveance series DPX-200 (200 MHz) spectrometer; the chemical shifts are reported in parts per million (ppm) relative to tetramethylsilane (TMS) as an internal standard. Elemental analyses were carried out using a Eurovector EA3000 series CHNOS analyser. Mass spectra were recorded on a Jeol-JMS-600H spectrometer in FAB$^+$ mode using 3-nitrobenzyl alcohol as a liquid matrix.

Mesophases were identified and their transition temperatures determined using a polarizing microscope (Leitz DMRXP) in conjunction with a programmable hot stage (Mettler FP90). Melting points of crystalline compounds were determined by the same system. The enthalpies of phase transition were measured using a differential scanning calorimeter (Perkin-Elmer DSC7) calibrated using indium as standard. Thermograms were recorded for two heating and cooling cycles at a rate of 5°C min^{-1}. Optical observations were made with either clean untreated glass slides or slides treated for homogeneous or homeotropic alignment of the molecules. X-ray diffraction studies were carried on powder samples in Lindemann capillaries with CuK radiation using an Image Plate Detector (MAC Science, Japan) equipped with double mirror focusing optics.

6.2. *Synthesis*

6.2.1. 4-Bromo-1-(1*S*-methylheptyloxy)-2-nitrobezene (7a). To a cooled (10–15°C) and magnetically stirred solution of 4-bromo-2-nitrophenol (1.0 g, 4.58 mmol, 1 equiv), (*R*)-2-octanol (0.72 g, 5.49 mmol, 1.2 equiv) and triphenylphosphine (1.4 g, 5.5 mmol, 1.2 equiv) in dry THF (5 ml) was added diethylazodicarboxylate (0.9 ml, 5.5 mmol, 1.2 equiv) dropwise over a period of 5 min. under an argon atmosphere. The reaction mixture was allowed to attain room temperature and was then stirred for 12 h. The solvent was removed *in vacuo* followed by the addition of ether (30 ml × 2). The organic layer was washed with 5% aqueous NaOH, 1N HCl, water (30 ml × 2), brine (30 ml) and was then dried over anhyd. Na_2SO_4. The evaporation of solvents furnished a crude oil, which was purified by column chromatography using silica gel (230–400 mesh). Elution with a mixture of 10% CH_2Cl_2 hexane afforded a colourless oil, R_f=0.54 in 15% CH_2Cl_2 hexane; yield 1.06 g (70%)). IR (neat): ν_{max} 2931, 2874, 1531 cm^{-1}. ^{1}H NMR (200 MHz, $CDCl_3$): δ 7.9 (d, J=2.5 Hz, 1H, Ar), 7.57 (d, J=6.5, 1H, Ar), 6.95 (d, J=9.0, 1H, Ar), 4.51–4.42 (m, 1H, 1 × OCH), 1.77–1.27 (m, 13H, 5 × CH_2,1 × CH_3) and 0.87 (t, J=6.3, 3H, 1 × CH_3). MS (FAB$^+$): *m/z* for $C_{14}H_{20}NOBr$, calcd 329.06; found 330.4.

6.2.2. 4-Bromo-1-(1*S*-methylheptyloxy)-2-fluorobezene (7b). This compound was synthesized and purified following the methods described for **7a**. Quantities: 4-bromo-2-fluorophenol (0.5 g, 2.61 mmol, 1 equiv), (*R*)-2-octanol (0.4 g, 3.1 mmol, 1.2 equiv), triphenylphosphine (0.8 g, 3.2 mmol, 1.2 equiv), diethylazodicarboxylate (0.5 ml, 3.2 mmol, 1.2 equiv). A colourless oil, R_f=0.54 in 15% CH_2Cl_2 hexane; yield 0.82 g (80%). IR (neat): ν_{max} 2930, 2874, 1581 cm^{-1}. ^{1}H NMR (200 MHz, $CDCl_3$): δ 7.25–7.12 (m, 2H, Ar), 6.88–6.79 (m, 1H, Ar), 4.31–4.25 (m, 1H, 1 × OCH), 1.78–1.27 (m, 13H, 5 × CH_2, 1 × CH_3) and 0.87 (t, J=6.6 Hz, 3H, 1 × CH_3). MS (FAB$^+$): *m/z* for $C_{14}H_{21}FOBr$, calcd 302.2; found 302.6.

6.2.3. 4-(2*R*-methylbutoxy)iodobezene (7c). This compound was synthesized and purified following the methods described for **7a**. Quantities: 4-iodophenol

(1.5 g, 6.82 mmol, 1 equiv), (*R*)-2-methylbutanol (0.72 g, 8.18 mmol, 1.2 equiv), triphenylphosphine (2.1 g, 8.18 mmol, 1.2 equiv), diethylazodicarboxylate (1.3 ml, 8.18 mmol, 1.2 equiv). A colourless oil; yield 1.56 (78%). IR (neat): ν_{max} 2961, 2874, 1586 cm^{-1}. ^1H NMR (400 MHz, $CDCl_3$): δ 7.53 (d, J=8.0 Hz, 2H, Ar), 6.7 (d, J=8.0, 2H, Ar), 3.9 (m, 2H, $1\times OCH_2$), 1.88–1.2 (m, 3H, $1\times CH$, $1\times CH_2$), 0.99 (d, J=6.8, 3H, $1\times CH_3$) and 0.93 (d, J=7.6, 3H, $1\times CH_3$). MS (FAB^+): *m*/*z* for $C_{11}H_{15}IO$, calcd 290; found 289.8.

6.2.4. (*S*)-1-(3,7-dimethyloctyloxy)-4-iodobenzene (7d). A mixture of 4-iodophenol (2.26 g, 10.3 mmol, 1 equiv.), (*S*)-1-bromo-3,7-dimethyloctane (2.7 g, 12.4 mmol, 1.2 equiv.), potassium carbonate (7.1 g, 51.5 mmol, 5 equiv.), potassium iodide (catalytic amount) and acetone was heated under refluxed for 12 h. The reaction mixture was filtered when hot, and the filtrate evaporated to dryness. The crude product was dissolved in CH_2Cl_2 and washed with water (30 ml × 2), brine (30 ml), then dried over anhydrous Na_2SO_4. Evaporation of CH_2Cl_2 furnished a crude oil that was purified by column chromatography using neutral alumina. Elution with a mixture of 5% CH_2Cl_2 hexane afforded a colourless oil, R_f=0.54 in 15% CH_2Cl_2 hexane; yield 2.68 g (72 %). IR (neat): ν_{max} 2953, 2860, 1587 cm^{-1}. ^1H NMR (400 MHz, $CDCl_3$): δ 7.53 (d, J=8.96 Hz, 2H, Ar), 6.67 (d, J=9.0, 2H, Ar), 3.96–3.89 (m, 2H, $1\times OCH_2$), 2.17–1.01 (m, 10H, $2\times CH$, $4\times CH_2$), 0.92 (d, J=6.52, 3H, $1\times CH_3$) and 0.86 (t, J=6.64, 6H, $2\times CH_3$). MS (FAB^+): *m*/*z* for $C_{16}H_{25}IO$, calcd 360; found 360.

6.2.5. (*S*)-2-Methyl-4-[3-nitro-4-(octan-2-vloxy)phenyl)]-but-3-yn-2-ol (6a). A mixture of compound **7a** (1.28 g, 3.88 mmol, 1 equiv.), 2-methyl-3-butyn-2-ol (0.424 g, 5.0 4mmol, 1.3 equiv.), bis(triphenylphosphine)palladium-(II) chloride (0.01 equiv.), triphenylphosphine (0.04 equiv.), and copper(I) iodide (0.04 equiv.) in dry triethylamine (5 ml) and dry THF (5 ml) was heated under reflux under argon for 16 h. The reaction mixture was cooled and filtered through a celite bed. The filtrate was evaporated *in vacuo* to give a pale yellow oil, which was purified by column chromatography using silica gel (100–200 mesh). Elution with a mixture of 10% EtOAc hexane furnished a colourless oil, R_f=0.38 in 20% EtOAc hexane; yield 1.04 g (80%). IR (neat): ν_{max} 3361, 2931, 2859, 1615, 1537 cm^{-1}. ^1H NMR (200 MHz, $CDCl_3$): δ 7.83 (d, J=2.0 Hz, 1H, Ar), 7.50 (d, J=8.0, 1H, Ar), 6.97 (d, J=8.0, 1H, Ar), 4.55–4.45 (m, 1H, $1\times OCH$), 1.96 (s,1H, $1\times OH$), 1.61–1.28 (m, 19H, $3\times CH_3$, $6\times CH_2$), and 0.88 (t, J=7.6 Hz, 3H, $1\times CH_3$). MS (FAB^+): *m*/*z* for $C_{19}H_{27}NO_4$, calcd 333.1; found 333.7.

6.2.6. (*S*)-2-Methyl-4-[3-fluoro-4-(octan-2-vloxy)phenyl]-but-3-yn-2-ol (6b). This compound was synthesized and purified following the method described for **6a**. Quantities: compound **7b** (1 g, 3.3 mmol, 1 equiv.), 2-methyl-3-butyn-2-ol (0.42 g, 4.95 mmol, 1.5 equiv.), bis-(triphenylphosphine)palladium(II) chloride (0.01 equiv.), triphenylphosphine (0.04 equiv.), copper(I) iodide (0.04 equiv.). A colourless oil, R_f=0.38 in 20% EtOAc hexane; yield 0.73 g (72%). IR (neat): ν_{max} 3625, 2930, 2859, 1581, 1494 cm^{-1}. ^1H NMR (200 MHz, $CDCl_3$): δ 7.55–7.32 (m, 1H, Ar), 7.15 (d, J=8.7 Hz, 1H, Ar), 6.83 (d, J=8.7, 1H, Ar), 4.31–4.26 (m, 1H, $1\times OCH$), 1.61–1.28 (m, 20H, $3\times CH_3$, $6\times CH_2$, $1\times OH$), and 0.87 (t, J=6.6, 3H, $1\times CH_3$). MS (FAB^+): *m*/*z* for $C_{19}H_{27}FO_2$, calcd 306.2; found 306.8.

6.2.7. (*R*)-2-Methyl-4-[4-(2-methylbutoxy)phenyl]but-3yn-2-ol (6c). This compound was synthesized and purified following the methods described for **6a**. Quantities: compound **7c** (1.7 g, 5.86 mmol, 1 equiv.), 2-methyl-3-butyn-2-ol (0.64 g, 7.62 mmol, 1.3 equiv.), bis-(triphenylphosphine)palladium(II) chloride (0.01 equiv.), triphenylphosphine (0.04 equiv.), copper(I) iodide (0.04 equiv.). A colourless oil, R_f=0.38 in 20% EtOAc hexane; yield 1.24 g (85 %). IR (neat): ν_{max} 3352, 2964, 2964, 1606, 1510 cm^{-1}. ^1H NMR (200 MHz, $CDCl_3$): δ 7.34(d, J=8.0 Hz, 2H, Ar), 6.81 (d, J=8.0, 2H, Ar), 3.8–3.6 (m, 2H, $1\times OCH_2$), 1.83–0.84 (m, 16H, $4\times CH_3$, $1\times CH_2$, $1\times CH$, $1\times OH$). MS (FAB^+): *m*/*z* for $C_{16}H_{22}O_2$, calcd 246; found 246.1.

6.2.8. (*S*)-4-[4-(3,7-dimethyloctyloxy)phenyl]-2-methylbut-3yn-2-ol (6d). This compound was synthesized and purified following the methods described for **6a**. Quantities: compound **7d** (2.0 g, 5.55 mmol, 1 equiv.), 2-methyl-3-butyn-2-ol (0.56 g, 6.66 mmol, 1.2 equiv.), bis-(triphenylphosphine)palladium(II) chloride (0.01 equiv.), triphenylphosphine (0.04 equiv.), copper(I) iodide (0.04 equiv.). A colourless oil, R_f=0.38 in 20% EtOAc hexane; yield 2.2 g (68%). IR (neat): ν_{max} 3352, 2928, 2228, 1606, 1509 cm^{-1}. ^1H NMR (200 MHz, $CDCl_3$): δ 7.34(d, J=8.9 Hz, 2H, Ar), 6.82 (d, J=8.9, 2H, Ar), 4.01–3.94 (m, 2H, $1\times OCH_2$), 2.02–1.16 (m, 11H, $4\times CH_2$, $1\times OH$),1.60 (s, 6H, $2\times CH_3$), 0.92 (d, J=6.3, 3H, $1\times CH_3$) and 0.87 (t, J=6.6 Hz, 6H, $2\times CH_3$). MS (FAB^+): *m*/*z* for $C_{21}H_{32}O_2$, calcd 316.5; found 316.

6.2.9. (*S*)-4-Ethynyl-1-(2-methyloctyloxy)-2-nitrobenzene (5a). A mixture of protected phenylacetylene **6a** (1.3 g, 3.95 mmol, 1 equiv.), potassium hydroxide (0.55 g, 9.89 mmol, 2.5 equiv) and toluene (20 ml) was heated at reflux for one hour under argon atmosphere. The

solvent was evaporated to dryness *in vacuo* and the brown mass obtained was poured into ice-cold water (50 ml). The aqueous layer was extracted with hexane (10 ml × 2), brine and dried over anhyd. Na_2SO_4. Evaporation of solvent furnished a pale brown oil, which was purified by column chromatography using alumina (neutral). Hexane elution furnished a pale brown oil, R_f=0.27 in hexane; yield 0.3 g (30 %). IR (neat): ν_{max} 3316, 2928, 2856, 2107, 1604 cm^{-1}. ^1H NMR (200 MHz, $CDCl_3$): 7.90 (d, J=2.1 Hz, 1H, Ar), 7.58 (d, J=8.74, 1H, Ar), 7.00 (d, J=7.0, 1H, Ar), 4.56–4.47 (m, 1H, 1 × OCH), 3.06 (s, 1H, alkyne H), 1.73–1.27 (m, 13H, 5 × CH_2, 1 × CH_3) and 0.87(t, J=6.7, 3H, 1 × CH_3). MS (FAB^+): *m/z* for $C_{16}H_{21}NO_2$, calcd 275.2; found 276.2.

6.2.10. (*S*)-4-Ethynyl-2-fluoro-1-(2-methyloctyloxy)-benzene (5b). This compound was synthesized and purified following the methods described for **5a**. Quantities: protected acetylene **6b** (1.0 g, 3.45 mmol, 1 equiv.), potassium hydroxide (0.45 g, 7.93 mmol, 2.5 equiv). R_f=0.27 in hexane; yield 0.6 g (73)%. IR (neat): ν_{max} 3316, 2928, 2107, 1604 cm^{-1}. ^1H NMR (200 MHz, $CDCl_3$): 7.38–7.12 (m, 2H, Ar), 6.67 (m, 1H, Ar), 4.41–4.33 (m, 1H, 1 × OCH), 3.06 (s, 1H, alkyne H), 1.74–1.28 (m, 13H, 5 × CH_2, 1 × CH_3) and 0.87(t, J=6.9, 3H, 1 × CH_3). MS (FAB^+): *m/z* for $C_{16}H_{21}FO$, calcd 248.2; found 249.1.

6.2.11. (*R*)-1-Ethynyl-4-(2-methylbutoxy)benzene (5c). This compound was synthesized and purified following the methods described for **5a**. Quantities: protected acetylene **6d** (0.73 g, 2.96 mmol, 1 equiv.), potassium hydroxide (0.33 g, 5.93 mmol, 2.0 equiv). R_f=0.27 in hexane; yield 0.41 g (73 %). IR (neat): ν_{max} 3392, 2962, 2107, 1606 cm^{-1}. ^1H NMR (200 MHz, $CDCl_3$): 7.42 (d, J=8.0 Hz, 2H, Ar), 6.83 (d, J=8.74, 2H, Ar), 3.85–3.68 (m, 2H, 1 × OCH_2), 2.98 (s, 1H, alkyne H) and 1.59–0.9 (m, 9H, 1 × CH, 1 × CH_2, 2 × CH_3). MS (FAB^+): *m/z* for $C_{13}H_{16}O$, calcd 188; found 188.1.

6.2.12. (*S*)-1-(3,7-Dimethyloctyloxy)-4-ethyloctyloxy)-4-ethynylbenzene (5d). This compound was synthesized and purified following the methods described for **5a**. Quantities: protected **6c** (1.65 g, 5.22 mmol, 1 equiv.), potassium hydroxide (0.55 g, 10.44 mmol, 2.0 equiv). R_f=0.27 in hexane; yield 1.34 g (98%). IR (neat): ν_{max} 3317, 2918, 2107, 1606 cm^{-1}. ^1H NMR (200 MHz, $CDCl_3$): 7.41 (d, J=8.8 Hz, 2H, Ar), 6.83 (d, J=8.9, 2H, Ar), 4.02–3.95 (m, 2H, 1 × OCH_2), 2.98 (s, 1H, alkyne H), 1.84–1.09 (m, 10H, 2 × CH, 1 × CH_2, 4 × CH_3), 0.93 (d, J=6.4, 3H, 1 × CH_3 and 0.87 (d, J=6.6, 3H, 1 × CH_3). MS (FAB^+): *m/z* for $C_{18}H_{26}O$, calcd 258; found 259.1.

6.2.13. Cholesteryl 6-(4-iodophenoxy)hexanoate (4a). A mixture of cholesteryl 6-bromohexanoate (1.98 g, 3.55 m.mol, 1 equiv.), 4-iodophenol (0.78 g, 3.55 mmol, 1 equiv.), anhydrous K_2CO_3 (1.96 g, 14.2 mmol, 4 equiv.) and dry DMF (20 ml) was heated at 85°C for 16 h under argon. The hot reaction mixture was filtered through a celite bed. The filtrate was evaporated *in vacuo* to give solid residue, which was poured into water. The off-white solid separated was collected by filtration. It was purified by recrystallization from a mixture of CH_2Cl_2 ethanol (1/10) to give a white solid, R_f=0.45 in 10% EtOAc hexane; yield 2.1 g (84%), m.p. 122–123°C. IR (KBr Pellet): ν_{max} 2940, 2875, 1731, 1578 cm^{-1}. ^1H NMR (400 MHz, $CDCl_3$): δ 7.53 (d, J=8.9 Hz, 2H, Ar), 6.66 (d, J=8.4, 2H, Ar), 5.38 (brd, J=4.1, 1H, 1 × olefinic), 4.62 (m, 1H, 1 × CHOCO), 3.91 (t, J=6.3, 2H, 1 × OCH_2), 2.29 (m, 4H, 2 × allylic methylene), 2.04–1.1 (m, 32H, 13 × CH_2, 6 × CH), 1.01 (s, 3H, 1 × CH_3), 0.91 (d, J=6.5, 3H, 1 × CH_3), 0.87 (d, J=1.8, 3H, 1 × CH_3), 0.85 (d, J=1.7, 3H, 1 × CH_3) and 0.68 (s, 3H, 1 × CH_3). FAB Mass: 725.0 $[M+Na]^+$: Calcd for $C_{39}H_{59}IO_3$.

6.2.14. Cholesteryl 6-(4-bromo-2-nitrophenoxy)-hexanoate (4b). A mixture of cholesteryl 6-bromohexanoate (1.95 g, 3.55 mmol, 1 equiv), 4-bromo-2-nitrophenol (0.78 g, 3.55 mmol, 1 equiv) and anhydrous K_2CO_3 (2.4 g, 17.5 mmol, 5 equiv) in dry DMF was heated at 85°C for 16 h under argon. The reaction mixture was filtered hot through a celite bed. The filtrate was evaporated *in vacuo* to give a solid residue, which was poured into water. The off-white solid separated was collected by filtration, and purified by recrystallization from a mixture of CH_2Cl_2 ethanol (1/10) to give a white solid; R_f=0.45 in 10% EtOAc hexane; yield 60%, m.p. 100–102°C. IR (KBr pellet): ν_{max} 2930, 2867, 1741, 1557 cm^{-1}. ^1H NMR (500 MHz, $CDCl_3$): δ 7.95 (d, J=2.4 Hz, 1H, Ar), 7.6 (dd, J_1=8.9, J_2=2.5, 1H, Ar), 6.95 (d, J=8.9, 1H, Ar), 5.37 (brd, J=4.1, 1H, 1 × olefinic), 4.63 (m, 1H, CHOCO), 3.96 (t, J=6.1, 2H, 1 × OCH_2), 2.47 (m, 4H, 2 × allylic methylene), 2.3–0.98 (m, 34H, 6 × CH, 14 × CH_2), 1.01 (s, 3H, 1 × CH_3), 0.91 (d, J=6.5, 3H, 1 × CH_3), 0.87 (d, J=1.5, 3H, 1 × CH_3), 0.85 (d, J=1.4, 3H, 1 × CH_3) and 0.67 (s, 3H, 1 × CH_3).

6.2.15. General procedure for the preparation of the unsymmetrical dimers 1a-3. A mixture of cholesteryl 6-(aryl)hexanoates (**4a, b**) (1 equiv.), phenylacetylenes (1.3 equiv) (**5a–5d**), bis(triphenylphosphine)palladium-(II) chloride (0.006 equiv.), triphenyl phosphine (0.04 equiv.), triethylamine (5 ml) and dry THF (5 ml) was heated under reflux under argon for 12 h. The

reaction mixture was filtered hot through a celite bed. The filtrate was evaporated under vacuum and the crude pale yellow solid obtained was dissolved in CH_2Cl_2 (20 ml); the resultant solution was washed with 1N HCl (10×2 ml), 5% aqueous solution of NaOH (10×2 ml), water (10×2), brine and then was dried over anhyd. Na_2SO_4. Evaporation of solvent furnished a dull pale yellow solid which was purified by column chromatography using alumina (neutral). Elution with a mixture of 10% EtOAc hexanes furnished a white solid that was further purified by repeated recrystallization from a mixture of CH_2Cl_2 ethanol (1/10) until a constant isotropic temperature was obtained.

6.2.16. Cholesteryl 6-{4-[3-nitro-4-(2S-methylheptyloxy)-phenylethynyl]phenoxy}hexanoate (1a). Pale yellow solid; R_f=0.3 in 30% CH_2Cl_2 hexane; yield 0.47 g (77%). UV-Vis: λ_{max}=298 nm, ($\in = 3.4 \times 10^4$ L mol^{-1} cm^{-1}), 311 nm, ($\in = 2.8 \times 10^4$ L mol^{-1} cm^{-1}), 316 nm, ($\in = 2.7 \times 10^4$ L mol^{-1} cm^{-1}). IR (KBr Pellet): ν_{max} 2934, 2867, 1740, 1618, 1531 cm^{-1}. ^{1}H NMR (400 MHz, $CDCl_3$): δ 7.90 (d, J=2.1 Hz, 1H, Ar), 7.58 (dd, J=2.2,8.7 Hz, 1H, Ar), 7.42 (d, J=8.8 Hz, 2H, Ar), 7.00 (d, J=8.9 Hz, 1H, Ar), 6.85 (d, J=8.8 Hz, 2H, Ar), 5.37 (brd, J=3.7 Hz, 1H, 1 × olefinic), 4.65–4.50 (m, 1H, 1 × CHOCO), 4.50–4.49 (m, 1H, 1 × OCH), 3.97 (t, J=6.36, 2H, 1 × OCH_2), 2.31 (t, J=7.3, 4H, 2 × CH_3), 1.98–0.85 (m, 48H, 6 × CH, 18 × CH_2, 2 × CH_3), 1.01 (s, 3H, 1 × CH_3), 0.91 (d, J=6.6, 3H, 1 × CH_3), 0.87 (d, J=1.8, 3H, 1 × CH_3), 0.85 (d, J=1.8, 3H, 1 × CH_3) and 0.67 (s, 3H, 1 × CH_3). ^{13}C NMR (125 MHz, $CDCl_3$): δ 173.0, 159.4, 151.0, 140.6, 139.7, 136.3, 133.0, 128.3, 122.6, 115.7, 115.5, 114.6, 89.9, 85.6, 73.8, 67.7, 56.7, 56.1, 50.0, 42.3, 39.7, 39.5, 38.2, 36.9, 36.6, 36.2, 35.8, 34.5, 31.8, 31.7, 29.1, 28.8, 28.2, 28.0, 27.8, 25.6, 25.2, 24.7, 24.3, 23.8, 22.8, 22.5, 21.0, 19.5, 19.3, 18.7, 14.0, 11.8. MS (FAB$^+$): m/z for $C_{55}H_{79}NO_6$, calcd 849.6; found 849.3. Elemental analysis: calcd(found), C 77.7 (77.8), H 9.37 (9.22), N1.65(1.60)%.

6.2.17. Cholesteryl 6-{4-[3-fluoro-4-(2S-methylheptyloxy)-phenylethynyl]phenoxy}hexanoate (1b). Pale yellow solid, R_f=0.35 in 30% CH_2Cl_2 hexane; yield 0.42 g (74%). UV-Vis: λ_{max}=298 nm, ($\in = 3.7 \times 10^4$ L mol^{-1} cm^{-1}), 305 nm, ($\in = 3 \times 10^4$ L mol^{-1} cm^{-1}), 317 nm, ($\in = 3.3 \times 10^4$ L mol^{-1} cm^{-1}). IR (KBr pellet): ν_{max} 2934, 2859, 1613, 1730 1517 cm^{-1}. ^{1}H NMR (400 MHz, $CDCl_3$): δ 7.42 (d, J=7.2 Hz, 2H, Ar), 7.22–7.18 (m, 2H, Ar). 6.89 (t, J=9.1 Hz, 1H, Ar), 6.83 (d, J=6.7 Hz, 2H, Ar), 5.37 (brd, J=3.7 Hz, 1H, 1 × olefinic), 4.65–4.58 (m, 1H, 1 × CHOCO), 4.39–4.35 (m, 1H, 1 × OCH), 3.97 (t, J=5.1 Hz, 2H, 1 × OCH_2), 2.32 (t, J=6.0 Hz, 4H, 2 × CH_2), 1.99–0.86 (m, 48H, 6 × CH, 18 × CH_2, 2 × CH_3), 1.01 (s, 3H, 1 × CH_3), 0.91 (d, J=6.5, 3H, 1 × CH_3), 0.87 (d, J=1.6, 3H, 1 × CH_3), 0.85 (d, J=1.6, 3H, 1 × CH_3) and 0.67 (s, 3H, 1 × CH_3). ^{13}C NMR (125 MHz, $CDCl_3$): δ 172.9, 159.1, 151.8, 146.3, 139.7, 132.9, 132.2, 127.7, 122.6, 122.1, 119.4, 119.2, 117.2, 116.5, 115.2, 114.5, 88.7, 86.9, 73.8, 67.7, 56.7, 56.2, 50.1, 42.3, 39.7, 39.5, 38.2, 37.0, 36.6, 36.4, 36.2, 35.5, 31.9, 31.7, 29.2, 28.8, 28.2, 28.0, 27.8, 25.5, 25.3, 24.7, 24.2, 23.8, 22.7, 22.5, 21.0, 19.7, 19.3, 18.7, 15.6, 15.0, 13.9, 11.8. MS (FAB$^+$): m/z for for $C_{55}H_{79}FO_4$ calcd 822.6; found 821.9. Elemental analysis: calcd (found), C 80.2 (80.1), H 9.9 (9.8)%.

6.2.18. Cholesteryl 6-{4-[4-(2R-methylbutyloxy)phenylethynyl]phenoxy}hexanoate (2a). White solid, R_f=0.35 in 30% CH_2Cl_2 hexane; yield 0.37 g (85%). UV-Vis: λ_{max}=296 nm, ($\in = 3.6 \times 10^4$ L mol^{-1} cm^{-1}), 305 nm, ($\in = 2.9 \times 10^4$ L mol^{-1} cm^{-1}), 315 nm, ($\in = 2.9 \times 10^4$ L mol^{-1} cm^{-1}). IR (KBr pellet): ν_{max} 2935, 2868, 1738, 1532 cm^{-1}. ^{1}H NMR (400 MHz, $CDCl_3$): δ 7.42 (d, J=8.7 Hz, 4H, Ar), 6.85 (d, J=8.6 Hz, 2H, Ar), 6.83 (d, J=8.6 Hz, 2H, Ar), 5.37 (brd, J=4.5 Hz, 1H, 1 × olefinic), 4.65–4.57 (m, 1H, 1 × CHOCO), 3.96 (t, J=6.4, 2H, 1 × OCH_2), 3.84–3.72 (m, 2H, 1 × OCH_2), 2.31 (t, J=7.4, 4H, 2 × CH_2), 2.01–0.85 (m, 41H, 7 × CH, 14 × CH_2, 2 × CH_3), 1.01 (s, 3H, 1 × CH_3), 0.91 (d, J=6.5, 3H, 1 × CH_3), 0.87 (d, J=1.7, 3H, 1 × CH_3), 0.85 (d, J=1.7, 3H, 1 × CH_3) and 0.67 (s, 3H, 1 × CH_3). ^{13}C NMR (125 MHz, $CDCl_3$): δ 172.9, 159.0, 158.8, 139.7, 132.8, 122.6, 115.7, 115.6, 114.5, 88.0, 87.9, 73.8, 72.9, 67.7, 56.7, 56.2, 50.1, 42.3, 39.7, 39.5, 38.2, 37.0, 36.6, 36.2, 35.8, 34.7, 34.5, 31.9, 28.8, 28.2, 27.9, 27.8, 26.1, 25.5, 24.7, 24.3, 23.8, 22.7, 22.5, 21.0, 19.2, 18.7, 16.5, 11.8, 11.2. MS (FAB$^+$): m/z for $C_{52}H_{74}O_4$, calcd 762.56; found 762.0. Elemental analysis: calcd (found), C 81.8 (82.0), H 9.77 (9.67)%.

6.2.19. Cholesteryl 6-{4-[4-(2R-methylbutyloxy)phenylethynyl]2-nitro-phenoxy}hexanoate (2b). Pale yellow solid, R_f=0.35 in 30% CH_2Cl_2 hexane; yield 0.26 g (76%). UV-Vis: λ_{max}=297 nm. ($\in = 3 \times 10^4$ L mol^{-1} cm^{-1}), 315 nm, ($\in = 2.7 \times 10^4$ L mol^{-1} cm^{-1}), 311 nm, ($\in = 2.5 \times 10^4$ L mol^{-1} cm^{-1}). IR (KBr pellet): ν_{max} 2928, 2867, 1731 1536 cm^{-1}. ^{1}H NMR (400 MHz, $CDCl_3$): δ 7.95 (d. J=2.1 Hz, 1H, Ar), 7.60 (dd, J=2.1,8.6 Hz, 1H, Ar), 7.42 (d, J=8.8 Hz, 2H, Ar), 7.01 (d, J=8.8 Hz, 1H, Ar), 6.87 (d, J=8.8 Hz, 2H, Ar), 5.37 (brd, J=4.2 Hz, 1H, 1 × olefinic). 4.62–4.60 (m, 1H, 1 × CHOCO), 4.12 (t, J=6.2, 2H, 1 × OCH_2), 3.85–3.75 (m, 2H, 1 × OCH_2), 2.33–0.85 (m, 45H, 7 × CH, 16 × CH_2, 2 × CH_3), 1.01 (s, 3H, 1 × CH_3), 0.91 (d, J=6.5, 3H, 1 × CH_3), 0.87 (d, J=1.6, 3H, 1 × CH_3),

0.85 (d, J=1.6, 3H, 1 × CH_3) and 0.67 (s, 3H, 1 × CH_3). ^{13}C NMR (125 MHz, $CDCl_3$): 172.9, 159.7, 151.8, 139.7, 136.5, 133.0, 128.3, 122.6, 116.2, 114.7, 114.4, 90.2, 85.5, 73.9, 73.0, 69.5, 56.7, 56.2, 50.1, 42.3, 39.8, 39.5, 38.2, 37.0, 36.6, 36.2, 35.8, 34.7, 34.5, 31.9, 28.6, 28.2, 28.0, 27.8, 26.1, 25.4, 24.6, 24.3, 23.8, 22.8, 22.5, 21.0, 19.3, 18.7, 16.5, 11.8, 11.2. Elemental analysis: calcd (found), C 77.3 (77.5), H 9.10 (9.17), N1.73 (1.56)%.

6.2.20. Cholesteryl 6-{4-[4-(3(S),7-dimethyloctyloxy)-phenylethynyl]phenoxy}hexanoate (3). White solid, R_f=0.4 in 30% CH_2Cl_2 hexane; yield 0.43 g (73%). UV-Vis: λ_{max}=297 nm, ($\in = 4.5 \times 10^4$ L mol^{-1} cm^{-1}), 305 nm, ($\in = 3.7 \times 10^4$ L mol^{-1} cm^{-1}), 315 nm, ($\in = 3.9 \times 10^4$ L mol^{-1} cm^{-1}). IR (KBr pellet): ν_{max} 2940, 2867, 1730, 1515 c; ^{1}H NMR (400 MHz, $CDCl_3$): δ 7.42 (d, J=8.8 Hz, 4H, Ar), 6.86–6.82 (m, 4H, Ar), 5.37 (brd, J=4.4 Hz, 1H, 1 × olefinic), 4.65–4.57 (m, 1H, 1 × CHOCO), 3.98–3.95 (m, 4H, 2 × OCH_2), 2.31 (t, J=7.2, 4H, 2 × CH_2), 1.98–0.85 (m, 55H, 8 × CH, 19 × CH_2, 3 × CH_3), 1.01 (s, 3H, 1 × CH_3), 0.91 (d, J=6.6, 3H, 1 × CH_3), 0.87 (d, J=1.7, 3H, 1 × CH_3), 0.85 (d, J=2.2, 3H, 1 × CH_3) and 0.67 (s, 3H, 1 × CH_3). ^{13}C NMR (125 MHz, $CDCl_3$): δ 172.9, 159.0, 158.8, 139.7, 132.8, 122.6, 115.7, 115.6, 114.5, 88.0, 87.9, 73.8, 67.7, 66.4, 56.7, 56.2, 50.1, 42.3, 39.7, 39.5, 39.2, 38.2, 37.3, 37.0, 36.6, 36.1, 35.7, 34.5, 31.9, 29.9, 28.8, 28.2, 27.9, 27.8, 25.6, 24.7, 24.6, 24.2, 23.8, 22.7, 22.6, 22.5, 21.0, 19.6, 19.3, 18.7, 11.8. MS (FAB$^+$): m/z for $C_{57}H_{84}O_4$, calcd 832.6; found 832.0. Elemental analysis: calcd (found), C 82.2 (82.3), H 10.16 (10.25)%.

7. Conclusion

We have achieved the molecular design, synthesis and characterization of unsymmetrical liquid crystal dimers in which naturally occurring cholesterol as chiral entity is covalently linked to a diphenylacetylene mesogenic segment through a pentamethylenecarbonyl, –$(CH_2)_5$CO–, flexible spacer. Specifically, we have explored the possibility of stabilizing a wide thermal range smectic A (SmA) phase. For this purpose, substituents of the tolane mesogenic segments were varied and their effect on thermal behaviour studied.

A dimer, having a (*S*)-methylheptyloxy chain and a nitro group, exhibits the SmA phase over ~110°C thermal range, in addition to a short interval chiral nematic phase (N*). Its fluoro analogue stabilizes the SmA phase solely over a temperature range of about 155°C. This behaviour can be attributed to the proximity of the chiral centre to the tolane core, while the presence of a laterally substituted polar group perhaps disfavours the formation of other layered fluid structures. The other dimer possessing a (*S*)-2-methylbutyloxy chain displayed the N*, twist grain boundary (TGB) and SmA phases, as well as an unknown mesophase. The polar analogue of this dimer, having a nitro group near the central spacer, showed the N* and the SmA phases, the latter occurring over a broad thermal range. The fifth dimer of the series, containing a (3*S*)-3,7-dimethyloctyloxy chain, displayed the SmA and chiral smectic (SmC*) phases.

Electro-optic studies were carried out for the majority of the compounds exhibiting the SmA phase. Electrical switching, molecular tilt angle and spontaneous polarization as functions of temperature were also investigated in the SmC* phase. It was found that, although some of the molecular structural parameters are conducive to large dipolar coupling, the poor electro-optic performance of the mesophases can perhaps be attributed to the bulkiness (volume) of the cholesterol segment. It appears that a further investigation involving the synthesis of such dimers with variation in the length of the central alkylene spacer must be undertaken in order to test this speculation.

Acknowledgements

We are grateful to the late Prof. S. Chandrasekhar for many helpful discussions. I. S. wishes to thank the Council of Scientific and Industrial Research (CSIR), for grant of a senior research fellowship. Financial support by CSIR, No. 01(1727)/02/EMR-II, is gratefully acknowledged.

References

[1] (*a*) C.T. Imrie, P.A. Henderson. *Curr. Opin colloid interface. Sci.*, **7**, 298, (2002); (*b*) C. T. Imrie. In *Structure and Bonding in Liquid Crystals II*, D. M. P. Mingos (Ed), p. 149, Springer-Verlag (1999); (*c*) C. T. Imrie, G. R. Luckhurst. In *Handbook of Liquid Crystals*, Vol 2B, D. Demus, J. W. Goodby, G. W. Gray, H. -W. Spiess, V. Vill, (Eds) p. 799, Wiley-VCH (1998).

[2] A.C. Griffin, T.R. Britt. *J. Am. chem. Soc.*, **103**, 4957 (1981).

[3] F. Hardouin, M.F. Achard, J.-I. Jin, J.-W. Shin, Y.K. Yun. *J. Phys II Fr.*, **4**, 267 (1994).

[4] F. Hardouin, M.F. Achard, J.-I. Jin, J.-W. Shin, Y.K. Yun. *J. Phys II Fr.*, **5**, 927 (1995); F. Hardouin, M. F. Achard, J.-I. Jin, J.-W. Shin, Y. K. Yun, S. J. Chung. *Eur. Phys. J.*, **B1**, 47 (1998); S.-W. Cha, J.-I. Jin, M. Laguerre, M. F. Achard, F. Hardouin. *Liq. Cryst*., **26**, 1325 (1999).

[5] S.W. Cha, J.-I. Jin, M.F. Achard, F. Hardouin. *Liq. Cryst.*, **29**, 755 (2002).

[6] J.-W. Lee, Y. Park, J.-I. Jin, M.F. Achard, F. Hardouin. *J. mater. Chem.*, **103**, 4957 (2003).

[7] K.-N. Kim, E.-D. Do, Y.-W. Kwon, J.-I. Jin. *Liq. Cryst.*, **32**, 229 (2005).

[8] V. Ajay Mallia, N. Tamaoki. *Chem. Mater.*, **15**, 3237, (2003) and references therein.

[9] A.T.M. Mercelis, A. Koudijs, Z. Karczmarzyk, E.J.R. Sudholter. *Liq. Cryst.*, **30**, 1357 (2003) and references therein.
[10] V. Surendranath. *Mol. Cryst. liq. Cryst.*, **332**, 135 (1999).
[11] C.V. Yelamaggad. *Mol. Cryst. liq. Cryst.*, **326**, 146 (1999).
[12] D.S. Shankar Rao, S. Krishna Prasad, V.N. Raja, C.V. Yelamaggad, S. Anitha Nagamani. *Phys. Rev. Lett.*, **87**, 085540 (2001).
[13] C.V. Yelamaggad, S. Anitha Nagamani, D.S. Shankar Rao, S. Krishna Prasad, U.S. Hiremath. *Mol. Cryst. liq. Cryst.*, **363**, 1 (2001).
[14] (*a*) S. Garoff, R.B. Meyer. *Phys. Rev. Lett.*, **38**, 848 (1997); (*b*) S. T. Lagerwall. In *Handbook of Liquid Crystals*, edited by D. Demus, J. Goodby, G.W. Gray, H. W. Spiess and V.Vill (Eds), Wiley-VCH, Weinheim (1998).
[15] G. Anderson, I. Dahl, W. Kuczynski, S.T. Lagerwall, K. Skarp, B. Stebler. *Ferroelectrics*, **84**, 285 (1988).
[16] N.A. Clark, S.T. Lagerwall. *Appl. Phys. Lett.*, **36**, 899 (1980).
[17] (*a*) C. Bahr, G. Heppke, U. Klemke. *Ber. Bunsenges. Phy. Chem.*, **95**, 761 (1991); (*b*) B. R. Ratna, G. P. Crawford, S. Krishna Prasad, J. Naciri, P. Keller, R. Shashidhar. *Ferroelectrics*, **148**, 425 (1993); (*c*) B. R. Ratna, G. P. Crawford, J. Naciri, R. Shashidhar. *Proc. SPIE.*, **2175**, 79 (1994).
[18] P.A. Williams, N.A. Clark, M. Blanca Ros, D.M. Walba, M.D. Wand. *Ferroelectrics*, **121**, 143 (1991).
[19] D.M. Walba, D.J. Dyer, R. Shao, N.A. Clark, R.T. Vohra, K. More, W.N. Thurmes, W.D. Wand. *Ferroelectrics*, **148**, 435 (1993).
[20] M. Redmond, H. Coles, E. Wischerhoff, R. Zentel. *Ferroelectrics*, **148**, 323 (1993).
[21] D. Guillon, M.A. Osipov, S. Mery, M. Siffert, J.-F. Nicoud, C. Bourgogne, P. Sebastio. *J. mater. Chem.*, **11**, 2700 (2001).
[22] (*a*) I. Nishiyama, J. Yamamoto, J.W. Goodby, H. Yokoyama. *J. mater. Chem.*, **11**, 2690 (2001); (*b*) I. Nishiyama, J. Yamamoto, J. W. Goodby, H. Yokoyama. *J. mater. Chem*., **12**, 1709 (2002).
[23] J.W. Goodby, J.A. Haley, G. Mackenzie, M.J. Watson, D. Plusquellec, V. Ferrieres. *J. mater. Chem.*, **5**, 2209 (1995).